

The tetrathienoanthracene (TTA) framework is explored as a star-shaped core that extends π -conjugation in two dimensions. The effect of “expanding” the conjugation by lengthening the oligothiophene side

chains is demonstrated with enhanced optoelectronic properties. Compared with its more flexible benzene analogue, the TTA derivatives show smaller band gaps and tight π -stacked structures.

A. A. Leitch, K. A. Stobo, B. Hussain,
M. Ghoussoub, S. Ebrahimi-Takalloo,
P. Servati, I. Korobkov,
J. L. Brusso* 1–11

Oligothiophene-Functionalized Benzene and Tetrathienoanthracene: Effect of Enhanced π -Conjugation on Optoelectronic Properties, Self-Assembly and Device Performance 

Keywords: Semiconductors / Pi interactions / Substituent effects / Molecular devices / Conducting materials

DOI: 10.1002/ejoc.201300731

Oligothiophene-Functionalized Benzene and Tetrathienoanthracene: Effect of Enhanced π -Conjugation on Optoelectronic Properties, Self-Assembly and Device Performance

Alicea A. Leitch,^[a,b] Kimberly A. Stobo,^[a,b] Bashir Hussain,^[a,b] Mireille Ghoussoub,^[c] Saeedeh Ebrahimi-Takaloo,^[c] Peyman Servati,^[c] Iliia Korobkov,^[a] and Jaclyn L. Brusso*^[a,b]

Keywords: Semiconductors / π interactions / Substituent effects / Molecular devices / Conducting materials

The versatility of fourfold Stille coupling to afford oligothiophene-functionalized tetrathienoanthracene (TTA) and benzene derivatives is described. The influence of the larger, more rigid TTA core on the electronic and structural properties was investigated. Comparative optical and electrochemical studies demonstrate a diminishing HOMO–LUMO gap as the length of the oligothiophene chain increases, with the rigid TTA compounds exhibiting lower energy gaps than the more flexible benzene analogues. X-ray crystallography studies reveal that the thiophene-substituted TTA structure

consists of slipped π -stacks with several close intrastack π – π interactions; no close contacts are observed for the benzene derivative due to twisting of the thiophene ligands out of plane. Consequently, the molecules in the benzene analogue are isolated from their neighbours. The thiophene and bithiophene functionalised TTA compounds were fabricated into OTFT devices in bottom-contact configuration and exhibited mobilities of ca. 10^{-4} cm² V⁻¹ s⁻¹ and on/off ratios of more than four orders of magnitude.

Introduction

In recent years, organic semiconductors (OSC) have seen significant development in part due to their potential use in optoelectronic device applications. Such interest stems from the ability to tune the electronic/optical properties, coupled with the desirable characteristics of plastics (versatility of chemical synthesis, mechanical flexibility, light weight, simple and low-cost processing) and, in the case of small molecule OSCs, well-defined molecular structures. These attractive features, which are observed in both polymeric and molecular materials, are the driving force behind the development of new and modified π -conjugated materials.^[1,2] However, in addition to chemical structure, organization of organic charge-transport materials is of utmost importance because their electronic properties are critically dependent on the extent of molecular order.^[3] The ability to transport charge is therefore vital to the implementation of molecular materials into next-generation electronic devices.

With respect to polymeric materials, the majority consist of one-dimensional (1D) chains in which delocalization occurs through the polymer backbone. Although this facilitates efficient transport of charge carriers and excitons along the chain, it leads to largely anisotropic charge mobility. Although crystallinity in polymer films may be observed in some cases [e.g., regioregular poly(3-hexylthiophene)], the inclusion of solubilizing groups can lead to disorder in the bulk, resulting in twisting of the polymer backbone and subsequent diminishing of the effective conjugation.^[4] This, coupled with the anisotropic charge mobility commonly observed in 1D conjugated polymers, limits the total electronic communication. Small molecule OSCs offer an attractive alternative to polymer-based systems because well-defined molecular structures may lead to a greater degree of order within the bulk. A particularly important requirement for the realization of high performance thin film optoelectronic devices for molecular materials is tight π -stacking interactions, which provide a pathway for charge transport. For example, field-effect transistors (FETs) based on small molecules (e.g., pentacene)^[5] generally attain higher mobilities than polymer-based devices owing to the crystallinity and, hence, morphology of the OSC. Unfortunately, the stability of higher oligoacenes under ambient conditions proves problematic for device operation and durability and provides the impetus to develop stable alternatives.^[6] To this end, incorporation of heteroatoms into an acene framework offers an opportunity to not only vary the physical and electronic properties, but also contribute

[a] Department of Chemistry, University of Ottawa, Ottawa, ON K1N 6N5, Canada
E-mail: jbrusso@uottawa.ca
Homepage: <http://mysite.science.uottawa.ca/jbrusso/index.html>

[b] Centre for Catalysis Research and Innovation, University of Ottawa, Ottawa, ON K1N 6N5, Canada

[c] Department of Electrical and Computer Engineering, University of British Columbia, Vancouver, BC V6T 1Z4, Canada

Supporting information for this article is available on the WWW under <http://dx.doi.org/10.1002/ejoc.201300731>.

to improved stability. This is accomplished through lowering of the HOMO energy levels thus making the system less susceptible to air oxidation under ambient conditions.^[6] It is also expected that inclusion of sulfur into an extended π -conjugated molecular framework will enhance intermolecular interactions, because it possesses a larger atomic orbital than carbon. This can significantly improve intermolecular communication in the solid state, which is necessary to facilitate carrier transport.^[1] In that regard, many thienoacene-based small molecule semiconductors have been developed, and, in fact, have contributed significantly to the development of high-performance organic field-effect transistors showing mobilities higher than $1.0 \text{ cm}^2 \text{ V}^{-1} \text{ s}^{-1}$.^[1,7]

To further improve the performance of thienoacene OSCs, a number of research groups have focused on increasing the dimensionality by extending the π -conjugation in two dimensions. It is anticipated that this approach will enhance the degree of intermolecular communication due to the larger conjugated framework while maintaining the increased stability afforded by the heteroatoms.^[8,9] The development of “star-shaped” conjugated molecules, in which the dimensionality is extended through a central core unit, has been shown to afford materials with physical properties that can be markedly different from their simple, linearly conjugated analogues.^[10] In recent years, a number of studies have been carried out in which a variety of core moieties have been implemented to increase the dimensionality of the OSCs (Figure 1).^[11–13] In general, tight π -stacking interactions are observed when substituents are attached to a rigid core [e.g., trithienothiophene (**3**)^[13] or dibenzothienotetrathienoanthracene (**4**)^[11]].

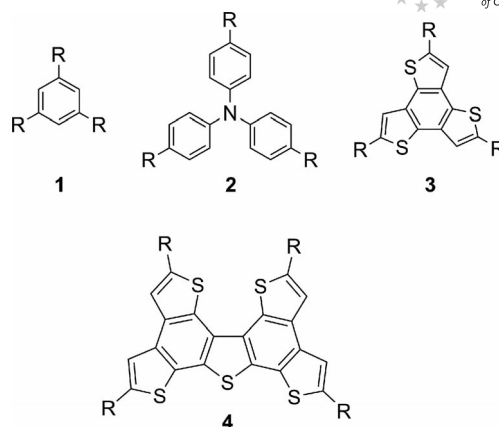


Figure 1. Star-shaped core moieties that can lead to increased dimensionality in OSCs.

In that regard, tetrathienoanthracene [TTA (**5c**), Figure 2] represents an ideal structure for use as the core moiety in star-shaped conjugated materials.^[9,14–16] Not only does it possess a planar, delocalized π -electron system, it has also been shown to form a highly organized 2D thin-film network and exhibits high thermal stability in air.^[14] Recently, we reported the preparation and characterization of halogenated (**5d**) and 5-hexyl-2-thienyl functionalized (**6a**) tetrathienoanthracene.^[15] It was demonstrated that increasing the effective conjugation of the thienoacene core enhanced the optoelectronic properties and led to a greater number of close intermolecular contacts. Continuing with this approach to “widening” the degree of conjugation and

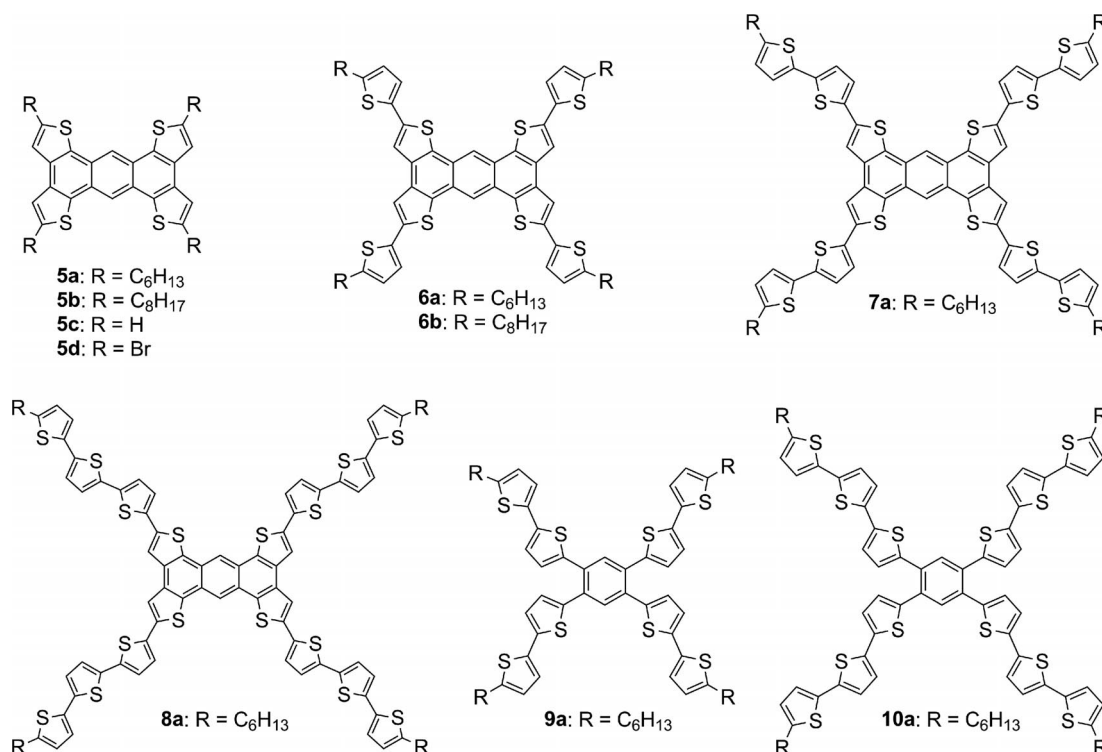


Figure 2. A family of oligothiophene-functionalized tetrathienoanthracene and benzene derivatives.

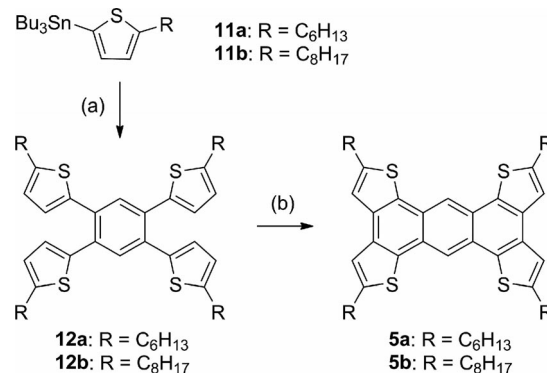
to investigate the versatility of the synthetic methodology, we herein report the preparation and characterization of bithiophene (**7a**) and terthiophene (**8a**) functionalized tetra-thienoanthracene. The benzene derivatives **9a** and **10a** were also isolated to compare the effect on the optoelectronic properties and solid-state structure between the rigid TTA cores to that of uncyclized analogues (i.e., the benzene core). Furthermore, in addition to augmenting the oligothiophene functionality, we also sought to investigate the effect of increased alkyl chain length. Although extension of the alkyl chain is expected to have little effect on the molecular properties, it is anticipated to have an impact on the solid-state structure as well as affording increased solubility. As such, the octylated derivatives **5b** and **6b** were isolated. Comparative studies by using cyclic voltammetry, UV/Vis and fluorescence spectroscopy were performed to illustrate the enhanced optoelectronic properties associated with “expanding” the conjugation of the TTA core. The solid-state structures of **6b** and **9a** were studied by X-ray crystallography, which revealed an increase in the number of close π - π contacts for **6b** compared with **6a** and demonstrated that tight π -stacking interactions are favoured for rigid cores over nonrigid systems (i.e., **9a**). We also report preliminary studies of the thin-film FETs of **6a** and **7a**.

Results and Discussion

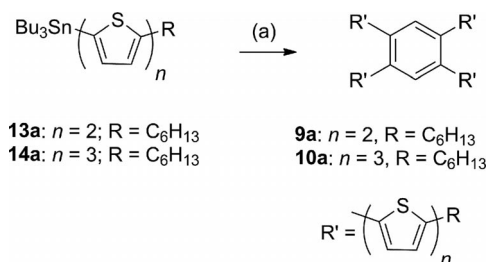
Synthesis

Our initial attempts to prepare oligothiophene-functionalized TTA focused on fourfold Stille coupling of tetrabromobenzene with stannylated oligothiophenes followed by oxidative cyclodehydrogenation with FeCl_3 .^[14,17] As outlined in Scheme 1, this route was effective for alkylated thiophene substituted benzene (i.e., in the preparation of **5a** and **5b**); however, when oligothiophenes such as bithiophene or terthiophene were used, an uncharacterizable solid was obtained. This may be attributed to the electron-donating character of the alkylated oligothiophenes, which facilitates side reactions of the β -thienyl positions generating a complex mixture of materials.^[17,18] Although oligothiophene-functionalized TTA was not accessible through this synthetic procedure, benzene analogues **9a** and **10a** were iso-

lated, leading to materials that could then be used for comparative purposes (Scheme 2). Bright-yellow plates of **9a** that were suitable for X-ray work were obtained through recrystallization from ethanol/dichloroethane mixtures. In the case of **10a**, crystal growth proved difficult due to its limited solubility.

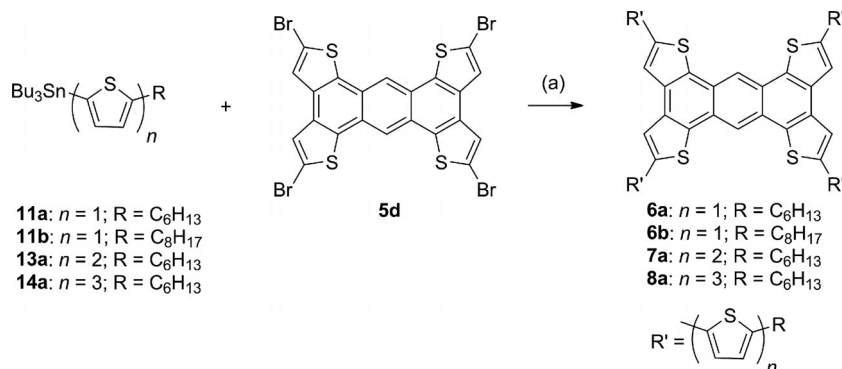


Scheme 1. Preparation of alkylated tetrathienoanthracene derivatives. *Reagents and conditions:* (a) 1,2,4,5-tetrabromobenzene, [Pd(PPh₃)₂Cl₂], DMF, 130 °C; (b) FeCl₃, MeNO₂/CH₂Cl₂, room temp.



Scheme 2. Preparation of the benzene derivatives **9a** and **10a**. *Reagents and conditions:* (a) 1,2,4,5-tetrabromobenzene, [Pd(PPh₃)₂Cl₂], DMF, 130 °C.

To overcome the synthetic challenges associated with oxidative cyclodehydrogenation of oligothiophene-functionalized benzenes, focus shifted to the preparation of the TTA core prior to functionalization. As described previously,^[15] 5-hexyl-2-thienyl functionalized TTA can be prepared through fourfold Stille coupling of 2-tributylstannyl-5-hex-



Scheme 3. Preparation of oligothiophene-functionalized TTA derivatives. *Reagents and conditions:* (a) [Pd(PPh₃)₂Cl₂], DMF, 130 °C.

ylthiophene (**11a**) with **5d** (Scheme 3). Although byproducts due to incomplete substitution were obtained, they can be removed through hot washes with ethyl acetate followed by recrystallization from dichloroethane. To demonstrate the versatility of this approach, fourfold Stille coupling of stannylated bithiophene (**13a**) and terthiophene (**14a**) with **5d** to afford **7a** and **8a** was carried out. Numerous attempts were made to afford single crystals of **7a** that were suitable for X-ray analysis; however, recrystallization only generated a microcrystalline solid. The challenges associated with crystal growth may be attributed to the diminished solubility related to extension of the π -conjugated framework; i.e., the hexyl chains became insufficient to overcome the strong π - π interactions. In the case of **8a**, purification from byproducts proved problematic; however, following Soxhlet extractions the desired material was observed in MALDI-TOF spectra. To address the diminished solubility associated with larger π -conjugated frameworks, octylated derivatives **5b** and **6b** were prepared according to the routes outlined in Schemes 1 and 3, respectively. We have therefore established a versatile route to alkylated oligothiophene functionalized benzene and tetrathienoanthracene. As demonstrated through the preparation of a series of compounds with differing core moieties, various oligothiophene lengths and augmented alkyl chains, this approach provides a facile method with which to modify π -conjugated materials.

Electrochemical, Spectroscopic and Computational Studies

To probe the influence of extended conjugation through oligothiophene-functionalization on the optoelectronic properties of tetrathienoanthracene and benzene based compounds, electrochemical and optical spectroscopy studies were performed on solutions of **5b**, **6b**, **7a**, **9a** and **10a** in dichloromethane; the results are summarized in Table 1. Cyclic voltammetry (CV) of **5b** and **6b** both revealed a single quasireversible redox process corresponding to the formation of the radical cation (see the Supporting Information). The oxidation potential of **6b** is shifted in the cathodic direction by 110 mV with respect to **5b** as a result of the enhanced conjugation length. Similar results were observed for the hexylated derivatives **5a** and **6a**; however, the

octylated derivatives exhibit more cathodic potentials than their hexylated analogues. Interestingly, the shift in oxidation potential observed upon further increasing the number of thiophene moieties attached to the TTA core was much less prevalent; a cathodic shift of only 20 mV was observed for the oxidation potential of **7a** compared with **6a** (cf. ca. 200 mV shift for **5a** \rightarrow **6a**). Furthermore, the CV of **7a** reveals two closely spaced irreversible oxidation waves and, upon repeated cycling, a coppery film appeared on the electrode. Although hexyl chains block the reactive sites on the terminal thiophene moieties, this may be attributed to polymerization at the β -thienyl positions on the oligothiophene arms following the formation of the radical cation species.

The benzene derivatives, **9a** and **10a**, exhibit similar redox behaviour, with two closely spaced oxidation waves separated by 80 and 140 mV, respectively, suggesting sequential formation of a radical cation and a dication. Because the separation between the first and second oxidation waves reflects the thermodynamic stability of the radical cation ($E_{1/2}^{2ox} - E_{1/2}^{1ox} = -0.059 \log K_{dispr}$),^[19] the greater potential difference between the first and second oxidation potentials for **10a** implies its radical cation is more thermodynamically stable than that of the less conjugated derivative **9a**. As may be expected, the rigidity associated with the TTA core leads to a more stable radical cation **7a**⁺ ($K_{dispr} = 1.3 \times 10^{-8}$) compared with the benzene derivatives **9a**⁺ ($K_{dispr} = 4.4 \times 10^{-2}$) and **10a**⁺ ($K_{dispr} = 5.2 \times 10^{-3}$).

It is interesting to note that similar shifts in oxidation potential were observed for the benzene analogues compared to the TTA derivatives with the same number of thiophene moieties. For example, **6a** and **9a** are both comprised of eight thiophene moieties, whereas **7a** and **10a** contain twelve. For both the benzene and TTA derivatives, a 20 mV shift in oxidation potential was observed upon increasing the number of thiophene moieties by four (e.g., **6a** \rightarrow **7a** and **9a** \rightarrow **10a**). Although the shifts in potential are similar, the oxidation potentials for the TTA analogues are more cathodic than the benzene derivatives. Thus, it may be inferred that the TTA derivatives should exhibit improved stability due to lower HOMO energy levels, making the system less susceptible to air oxidation under ambient conditions.^[6]

Table 1. Theoretical,^[a] electrochemical^[b] and photophysical^[c] properties.

	5a ^[d]	6a ^[d]	7a	9a	10a	5b	6b
$E_{HOMO}^{calcd.}$ [eV]	-5.21	-5.12	-5.08	-5.11	-5.03	-5.21	-5.12
$E_{gap}^{calcd.}$ [eV]	3.35	2.95	2.75	3.08	2.79	3.35	2.95
E^{ox1} [V]	1.15	0.94	0.92	1.07	1.05	1.02	0.91
E^{ox2} [V]			1.39	1.15	1.19		
E_{HOMO}^{expt} [eV] ^[e]	-5.33	-5.11	-4.89	-5.30	-5.25	-5.13	-4.98
λ_{max}^{abs} [nm]	431	475	437	356	395	431	475
λ_{edge}^{abs} [nm]	440	493	521	447	480	440	493
E_{gap}^{opt} [eV] ^[f]	2.83	2.52	2.38	2.77	2.58	2.83	2.52
λ_{max}^{PL} [nm] ^[g]	435	490	512	494	517	435	490
Stokes shift [eV]	0.03	0.08	0.42	0.97	0.74	0.03	0.08

[a] DFT/B3LYP/6-31G(d,p) level of theory where R = Me. [b] In CH_2Cl_2 , 0.1 M nBu_4NPF_6 as supporting electrolyte, referenced to the Fc/Fc^+ couple of ferrocene at +0.48 V vs. SCE.^[20] [c] Measurements performed in CH_2Cl_2 . [d] Data taken from ref.^[15] and provided here for comparison. [e] Derived using the following expression: $E_{HOMO} = -e(E^{ox} - E^{Fc/Fc^+} + 4.8)$.^[21] [f] Calculated from λ_{edge} . [g] In CH_2Cl_2 , upon excitation at 320 nm for **5a** and **5b**, 380 nm for **6a** and **6b**, 436 nm for **7a**, 356 nm for **9a**, and 396 nm for **10a**.

Optical spectroscopy provides further evidence of enhanced π -conjugation associated with augmented oligothiophene chain length. Comparison of the absorption and emission profiles for the TTA derivatives revealed a bathochromic shift as the oligothiophene chain length increased (i.e., 55 nm for **5a**→**6a**; 28 nm for **6a**→**7a**; see Table 1 and Figure 3), which is indicative of enhanced electronic delocalization. Although the absorption and emission profiles for **5a**, **6a** and **7a** are similar, peak broadening and loss of fine structure are observed upon increasing oligothiophene chain length. This may be attributed to a less rigid structure due to the flexibility of the oligothiophene substituents. As expected, the addition of thiophene moieties leads to a decrease in the optical energy gap, albeit to diminishing extents, upon elongating the oligothiophene arms (0.31 eV for **5a**→**6a**; 0.13 eV for **6a**→**7a**). Such observations have been noted elsewhere^[22] and are consistent with the trends observed in the redox potentials and DFT calculations (see below). Not surprisingly, the absorption and emission spectra for **5b** and **6b** are identical to that of **5a** and **6a**, respectively (see the Supporting Information, Figure S4).

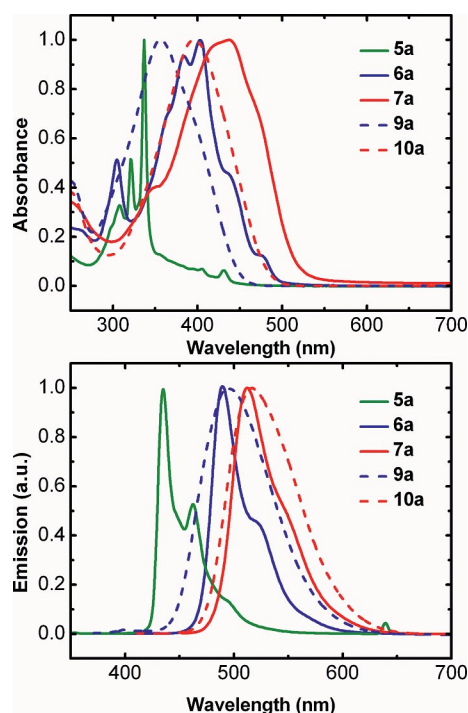


Figure 3. Absorption (top) and emission (bottom) spectra of **5a** (green solid line), **6a** (blue solid line) and **7a** (red solid line) as well as the benzene derivatives **9a** (blue dashed line) and **10a** (red dashed line).

The optical spectra of the benzene derivatives also provide evidence of increased effective conjugation associated with elongation of the oligothiophene groups. Bathochromic shifts of ca. 50 and 23 nm are observed in the absorption and emission spectra, respectively, for **10a** with respect to **9a** (see Table 1 and Figure 3). Based on the onset of UV/Vis absorption, a decrease in the optical energy gap is associated with an increase in the number of thiophene

moieties attached to the benzene core. This is consistent with an increase in conjugation and is similar to the shifts observed in the TTA analogues. Furthermore, the broader and less defined absorption and emission profiles for the benzene analogues compared with the TTA derivatives are attributed to the less rigid structure.^[17] These results are consistent with DFT geometry optimization calculations and crystal structure elucidation.

Comparison of the Stokes shifts reveals larger energies for the benzene derivatives compared with TTA based compounds; this may also be explained by molecular flexibility. The values obtained for **5a**, **5b**, **6a** and **6b** are quite promising when compared with other fused thienoacenes (e.g., 0.28 eV for pentathienoacene),^[23] because low Stokes shifts are indicative of little structural distortion upon excitation. This strongly suggests that the reorganization energy of the charge carrier (polaron or radical cation), which limits the intrinsic mobility of OSCs, will be low. The larger value obtained for **7a** may be attributed to the instability of the excited state, as observed for the radical cation in the CV, in addition to the potential flexibility afforded by the longer oligothiophene arms.

The overall bathochromic shifts upon functionalization suggests highly delocalized states with communication between the core moieties and oligothiophene substituents. To further explore the delocalized character, density functional theory (DFT) calculations at the B3LYP level with the 6-31G(d,p) basis set were performed. The HOMO contours (see the Supporting Information, Figure S5 and S6) illustrate that the electron density is distributed from the core out to the periphery along the oligothiophene substituents in both the TTA and benzene derivatives. Furthermore, as the number of thiophene rings increase, the calculated HOMO energy level rises as the HOMO–LUMO gap narrows, albeit to diminishing extents, upon elongating the oligothiophene moiety. This observation is consistent with the trends observed in the electrochemical and spectroscopic behaviour of these systems.

X-ray Crystallography

Because long-range molecular order and π -orbital overlap are of paramount importance to obtain high charge carrier mobilities in OSCs, the solid-state structures of **6b** and **9a** were studied by X-ray crystallography. It was recently demonstrated that extending the conjugation in two dimensions, through the attachment of 5-hexyl-2-thienyl moieties to a TTA core, favoured close π -stacking interactions,^[15] and contained a greater number of close π – π interactions compared with the protonated derivative **5c**. In addition to augmenting the oligothiophene functionality, we also sought to investigate the influence of increasing the alkyl chain length. As evidenced by optical spectroscopy, extension of the alkyl chain has little effect on the molecular properties; however, it was anticipated to have an impact on the solid-state structure. To this end, single crystals of **6b** were analysed by X-ray diffraction. Crystals of **6b** belong

to the triclinic space group $P-1$ and consist of slipped π -stacks running along the x -direction. Two views of the crystal structure, showing the unit-cell packing and the slipped π -stacked structure, are provided in Figure 4. Similar to **6a**, these molecules are essentially planar, with the core atoms showing minimal displacement from the mean plane of the 26-atom TTA core (0.0302 and 0.0213 Å for **6b** and **6a**, respectively). Interestingly, replacement of the hexyl chains with octyl substituents leads to twisting of the thiophene moieties attached to the TTA core. Whereas the hexylated derivative exhibits only a slight propeller-like distortion with relatively similar dihedral angles [4.3(4)° and 7.8(3)°], the octylated derivative displays two unique thiophene twist angles from the molecular plane; one significantly twisted [27.2(1)°] and the second relatively planar with the TTA core [6.20(1)°]. Furthermore, the octyl substituents in **6b** form an interdigitated network between the slipped π -stacks, similar to the hexyl chains in **6a**. Consequently, the degree of lateral communication is diminished in both materials.

Comparison of the slipped π -stacked structures of octylated versus hexylated thiophene functionalized TTA demonstrates the influence that larger substituents play on the packing pattern. It is interesting to note that inclusion of octyl substituents increased the number of close contacts within the π -stacked structure compared with the hexylated derivative **6a**.^[15] This is attributed to the steeply inclined slipped π -stacked structure; in order to accommodate the octyl chains the degree of slippage increases [30.94(1)° cf. 34.34(2)° for **6a**]. The larger degree of inclination, quantified in terms of the slippage angle (a smaller angle value indicates a higher degree of slippage), leads to a decrease in the interplanar separation between molecules [3.365(2) Å for **6a**; 3.361(2) Å for **6b**].^[15,24] Diminishing the interplanar separation results in an increase in the number of close contacts within the slipped π -stacks for **6b**, which are within or nominally larger than the van der Waals separation,^[25] as shown in Figure 4. The observation of a number of π - π contacts in **6b** may be attributed to the extended π -conjugated core; i.e., the potential for π - π interactions is increased due to the large molecular framework. It was therefore anticipated that **7a** should exhibit an even greater number of π - π interactions when similar π -stacking is observed; however, despite significant efforts, we were unable to obtain crystals of **7a** that were suitable for single-crystal X-ray analysis.

To shed light on the effect that a fused versus nonfused core has on supramolecular organization, single crystals of **9a** were analysed by X-ray diffraction and found to belong to the triclinic space group $P-1$. The bithiophene substituents are significantly twisted with respect to the benzene core due to steric interactions with the benzyl protons, and limited intermolecular communication is observed (see the Supporting Information, Figure S7). As a result, the only close contacts belong to the aliphatic substituents. This demonstrates the necessity for the fused thienoanthracene core to facilitate strong π - π interactions and overcome alkyl-alkyl interactions.

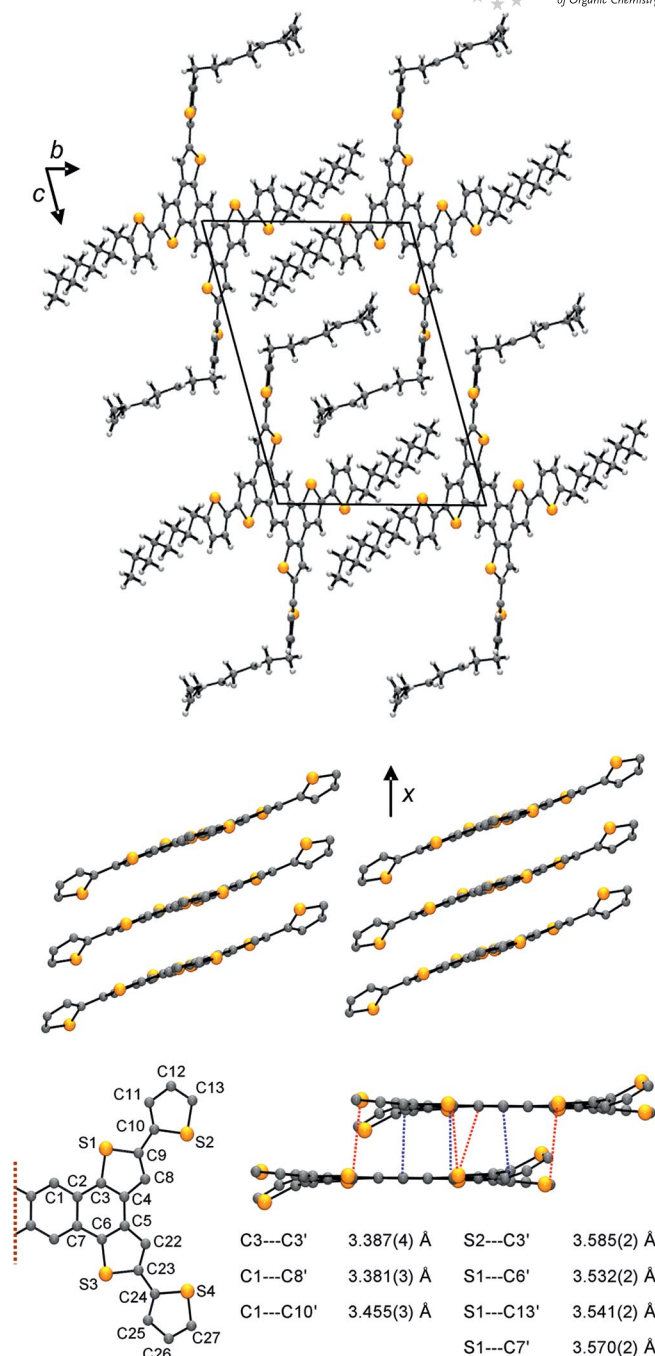


Figure 4. Unit cell (top), slipped π -stack (middle) drawings, and the crystal structure of **6b** showing atom numbering and close intermolecular contacts along the π -stack (bottom). In the π -stacked structure, octyl chains are omitted for clarity. C-C' contacts are shown in blue; S-C' are in red.

Band Structure Calculations

As the crystal structures of **6a** and **6b** illustrate, augmentation of alkyl chain length plays an important structural role with respect to the degree of slippage and interplanar separation within the slipped π -stacks. Such differences in molecular packing will clearly have an impact on the solid-state properties of these systems. To probe the electronic consequences of these differences, we carried out

extended Hückel theory (EHT) band structure calculations on the crystal structures of **6a**, **6b** and **9a** (see the Supporting Information, Figure S8). Such calculations have been very useful in understanding the electronic structure of organic molecular superconductors^[26] and thin-film field-effect transistors.^[27] The results suggest that **6a** and **6b** are indirect semiconductors, with calculated band gaps of 2.04 and 2.16 eV, respectively. These values correlate reasonably well with the experimentally obtained optical energy gap of 2.52 eV. Conversely, the band structure of **9a** reveals a direct semiconductor with a calculated band gap of 2.69 eV, a value that is comparable to the optical energy gap of 2.77 eV obtained experimentally.

Device Fabrication and Testing

To investigate the charge transport properties, bottom-contact configuration thin-film transistors (TFTs) were fabricated by spin-coating chlorobenzene solutions of **6a** and **7a** onto (100) silicon wafer substrates coated with 100 nm thermally grown SiO₂. Drain and source electrodes were patterned by electron beam evaporated gold in the form of interdigitated electrodes, as shown in the inset of Figure 5. The transfer current-voltage characteristics of **6a** and **7a** TFTs are illustrated in Figure 5, with a channel width to length ratio of 40000:50 measured at a drain source voltage of -37 V to ensure biasing in the saturation region. As can be seen, both devices exhibit more than four orders of magnitude on/off ratios. Devices with **7a** show a threshold voltage of around -6 V in comparison to -4 V for **6a** devices. Whereas the devices exhibit similar current levels, **7a** TFTs show slightly higher currents at high gate biases. Using the saturation current equation, the field effect mobility of these devices can be extracted as 5.2×10^{-4} and $6.0 \times 10^{-4} \text{ cm}^2\text{V}^{-1}\text{s}^{-1}$ for **6a** and **7a**, respectively.

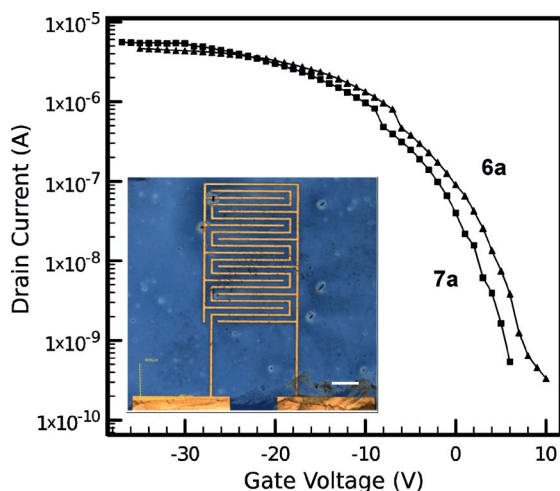


Figure 5. Drain current as a function of gate voltage for **6a** and **7a** TFTs with width to length ratio 40000:50, measured at drain-source voltage of -37 V. Inset illustrates the photomicrograph of interdigitated source and drain electrodes used in this measurement. Scale bar 50 μm .

The output characteristics of **6a** and **7a** TFTs are illustrated in Figure 6, whereby the drain current is measured as a function of drain voltage changing between 0 and -36 V for gate biases of -20 to 4 V with a step of 6 V. These figures demonstrate that both devices show a clear “pinch-off” point for transition from linear to saturation regions. In the saturation region, the current slowly increases with increasing negative gate voltage, as expected. To probe the effect of solution concentration on the device performance, two different chlorobenzene solutions for both **6a** and **7a** with concentrations of 8.3 and 6.25 mg/mL were prepared at 80 °C. From these studies, the best performance was determined to occur at a concentration of 8.3 mg/mL for both materials; however, the effect appears to be less significant for **7a** than for **6a** (see the Supporting Information, Figure S9).

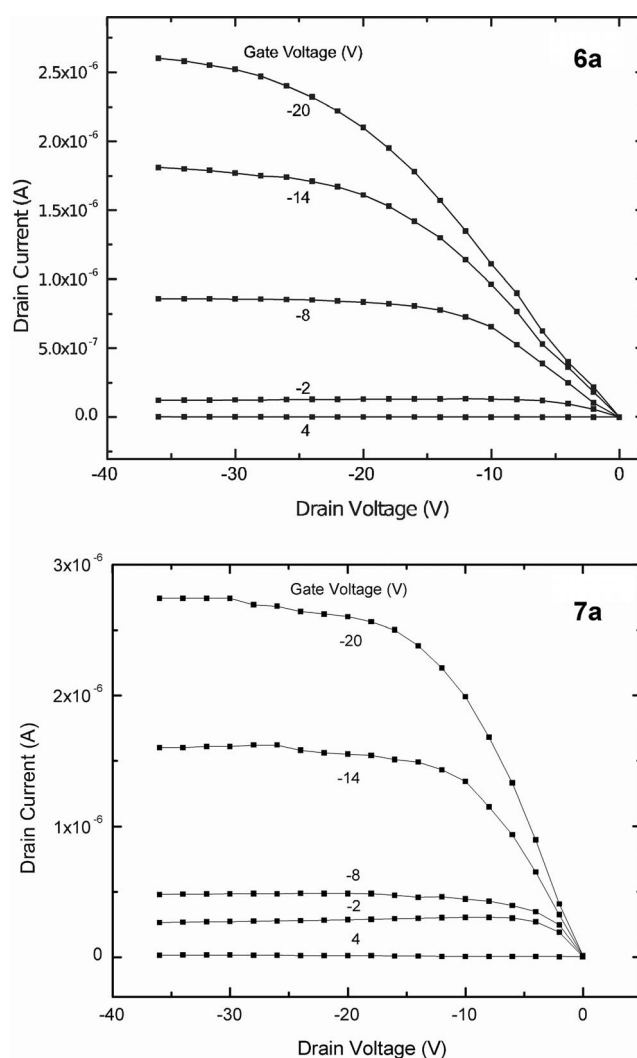


Figure 6. Output characteristics of **6a** (top) and **7a** (bottom) TFTs for different gate biases, showing a smooth transition from the linear to saturation regions.

The relatively modest mobilities obtained for **6a** and **7a** devices are comparable to that of drop-cast TFTs based on **5a** ($2.5 \times 10^{-4} \text{ cm}^2\text{V}^{-1}\text{s}^{-1}$; ON/OFF ratio 10^4)^[14] and may be attributed to the packing of the molecules in thin films.

Whereas favourable π - π interactions are observed in the single-crystal structures, these features may not translate to the thin film. Similar challenges associated with thin-film morphology have been reported for tetraphenyltetracene (rubrene), which exhibits a planar structure with strong π - π interactions and very high mobility in single crystals,^[28] however, fails to show any appreciable mobility in thin films due to the twisted geometry it adopts.^[29] Detailed structural/morphological analysis of thin films of these compounds is needed to fully elucidate these results. As demonstrated with **5a**, these values may be improved by fabricating devices by using vacuum sublimation methods ($1.9 \times 10^{-2} \text{ cm}^2 \text{ V}^{-1} \text{ s}^{-1}$; ON/OFF ratio 10^6).^[14]

Conclusions

The versatility of fourfold Stille coupling to afford a series of oligothiophene-functionalized benzene and tetrathienoanthracene materials has been demonstrated. The TTA framework can be used as a convenient building block to access extended planar delocalized π -electron systems. As may be expected, solubility becomes problematic as the π -conjugated framework is extended for the TTA derivatives; however, these solubility issues may be alleviated through the incorporation of longer chain and/or swallowtail alkyl substituents. Nonetheless, 5-hexyl-2-thienyl (**6a**) and 5'-hexyl-2,2'-bithien-5-yl (**7a**) functionalized tetrathienoanthracene, their benzene analogues **9a** and **10a**, as well as octylated derivatives **5b** and **6b** have been characterized by cyclic voltammetry, UV/Vis and fluorescence spectroscopy. These comparative studies illustrate the enhanced optoelectronic properties associated with "expanding" the conjugation of the aromatic core. The solid-state structures of **6b** and **9a** were studied by X-ray crystallography, which revealed an increase in the number of close π - π contacts for **6b** compared with that of **6a**, and demonstrated that tight π -stacking interactions are favoured for rigid cores over nonrigid systems (i.e., **9a**). Preliminary OTFT devices of **6a** and **7a** in bottom-contact configuration showed unoptimized mobilities of ca. $10^{-4} \text{ cm}^2 \text{ V}^{-1} \text{ s}^{-1}$ and on/off ratios of more than four orders of magnitude. Although these values are moderate, this may be attributed to the disorder associated with the spin-coating process at room temperature. Detailed structural/morphological analysis of thin films of these compounds may provide a more in-depth understanding of these results.

Experimental Section

General Procedures and Starting Materials: The reagents 1,2,4,5-tetrabromobenzene, palladium chloride and triphenylphosphane were obtained commercially and used as received. Compounds 5-(hexyl)-5'-(tributylstannyl)-2,2'-bithiophene (**13a**),^[30] 5-(hexyl)-5'-(tributylstannyl)-2,2':5',2''-terthiophene (**14a**),^[31] **5d**^[15] and 5-(octyl)-2-(tributylstannyl)thiophene (**11b**)^[32] were prepared as outlined in the literature. All solvents were of at least reagent grade; tetrahydrofuran (THF) was dried by distillation from sodium, and dimethylformamide (DMF) was dried with 4 Å molecular sieves. All

reactions were performed under an atmosphere of dry nitrogen. Melting points are uncorrected. ¹H and ¹³C NMR spectra were run in either CDCl₃ or C₂D₂Cl₄ solutions at room temp. or 50 °C with a Bruker Avance II 300 MHz spectrometer, a Bruker Avance 400 MHz spectrometer or a Bruker Avance 500 MHz Wide Bore spectrometer. Infrared spectra were recorded with a Bomem Hartmann & Braun MB-Series FTIR spectrometer using NaCl optics and a Nujol mull. UV/Vis spectra were measured with a Varian Cary-100 spectrophotometer and the fluorescence spectra were obtained with a Photon Technology International (PTI) spectrofluorimeter. Both UV/Vis and fluorescence spectra were measured on dichloromethane solutions with a 1 cm precision quartz cuvette. Elemental analyses were performed by MWH Laboratories, Phoenix, AZ, USA.

Electrochemistry: Cyclic voltammetry was performed with a Princeton Applied Research (PAR) VersaSTAT 3 potentiostat/galvanostat/frequency response analyser and V3-Studio electrochemical software [V 1.0.281 (c) 2008 PAR] employing a glass cell fitted with platinum electrodes. The measurements were carried out on dichloromethane solutions (dried by distillation over CaH₂) containing 0.1M tetrabutylammonium hexafluorophosphate (Aldrich) as supporting electrolyte with a scan rate of 100 mV/s. The experiments were referenced to the Fc/Fc⁺ couple of ferrocene at +0.48 V vs. SCE.^[20]

Crystal Growth: Crystals of **6b** that were suitable for X-ray analysis were grown by slowly cooling a saturated dichloroethane solution. Crystals of **9a** that were suitable for X-ray analysis were grown by recrystallization from an ethanol/dichloroethane solution.

X-ray Measurements: Crystals of **6b** and **9a** were mounted on thin glass fibres using paraffin oil. Data were collected at 200.15 K with a Bruker AXS KAPPA single-crystal diffractometer equipped with a sealed Mo tube source (wavelength 0.71073 Å) APEX II CCD detector. Raw data collection and processing were performed with the APEX II software package from BRUKER AXS.^[33] The structures were solved by direct methods, completed with difference Fourier synthesis, and refined with full-matrix least-squares procedures based on F^2 using the SHELXTL suite of programs. Disorder was observed in the alkyl chains of both compounds. Further details are provided in the Supporting Information.

Fabrication of Thin-Film Transistors: Thin-film transistors (TFTs) were fabricated by spin-coating solutions of **6a** and **7a** in chlorobenzene on (100) silicon wafer substrates coated with 100 nm thermally grown SiO₂. Moderately doped *p*-type wafer was used as the gate of the transistor and was contacted by a 200 nm Al film deposited on the back of the wafer. Drain and source electrodes were patterned by electron beam evaporated gold in the form of interdigitated electrodes having different channel length and width for several test devices. Compounds **6a** and **7a** were dissolved in chlorobenzene with a typical concentration of 6.25 mg/mL and stirred on a hotplate at 90 °C for 20 min and 2 h, respectively, before spin coating. All the samples were spin coated at 2000 rpm for 30 s.

Preparation of 9a: 1,2,4,5-Tetrabromobenzene (0.50 g, 1.27 mmol), PdCl₂ (22 mg, 0.124 mmol), PPh₃ (66 mg, 0.252 mmol) and **13a** (4.12 g, 7.64 mmol) were stirred in degassed DMF (0.2 mL) at 140 °C for 16 h. After cooling to room temp., diethyl ether was added and the crude product (0.98 g, 0.910 mmol, 72%) was filtered and washed with diethyl ether. Recrystallization from EtOAc afforded small yellow needles; crystals that were suitable for X-ray crystallography were obtained from ethanol/dichloroethane mixtures; m.p. >107 °C (dec.). ¹H NMR (CDCl₃, room temp., 400 MHz): δ = 7.62 (s, 2 H), 6.96 (d, J = 3.7 Hz, 4 H), 6.94 (d, J

= 3.5 Hz, 4 H), 6.85 (d, J = 3.7 Hz, 4 H), 6.64 (d, J = 3.6 Hz, 4 H), 2.76 (t, J = 7.5 Hz, 8 H), 1.65 (m, J = 7.5 Hz, 8 H), 1.41–1.27 (m, 24 H), 0.88 (t, J = 6.9 Hz, 12 H) ppm. ^{13}C NMR (CDCl_3 , room temp., 400 MHz): δ = 145.67, 139.62, 139.01, 134.74, 133.40, 132.83, 128.37, 124.92, 123.59, 123.28, 31.73, 31.72, 30.33, 28.90, 22.72, 14.24 ppm. IR: $\tilde{\nu}_{\text{max}}$ = 3064.3 (w), 1501.3 (m), 1239.2 (w), 1209.8 (w), 1191.9 (w), 1162.4 (w), 1057.2 (w), 1038.1 (w), 907.2 (w), 867.5 (m), 816.4 (s), 803.4 (s), 793.0 (s), 738.0 (w), 722.9 (w) cm^{-1} . $\text{C}_{62}\text{H}_{70}\text{S}_8$ (1071.72): calcd. C 69.48, H 6.58; found C 69.30, H 6.76.

Preparation of 10a: 1,2,4,5-Tetrabromobenzene (0.21 g, 0.533 mmol), PdCl_2 (9 mg, 0.0508 mmol), PPh_3 (28 mg, 0.107 mmol) and **14a** (2.00 g, 3.22 mmol) were stirred in degassed DMF (0.1 mL) at 130 °C for 16 h. After cooling to room temp., diethyl ether was added and the crude product (0.75 g, 0.538 mmol, 100%) was filtered and washed with diethyl ether. Recrystallization from DCE afforded an orange microcrystalline powder (0.65 g, 0.467 mmol, 88%); m.p. 196–198 °C. ^1H NMR ($\text{C}_2\text{D}_2\text{Cl}_4$, 50 °C, 300 MHz): δ = 7.71 (s, 2 H), 7.14–7.08 (m, 8 H), 7.05–7.01 (m, 8 H), 6.98 (d, J = 3.8 Hz, 4 H), 6.72 (d, J = 3.6 Hz, 4 H), 2.82 (t, J = 7.6 Hz, 8 H), 1.72 (m, J = 7.4 Hz, 8 H), 1.49–1.30 (m, 24 H), 0.93 (t, J = 6.7 Hz, 12 H) ppm. ^{13}C NMR ($\text{C}_2\text{D}_2\text{Cl}_4$, 50 °C, 300 MHz): δ = 145.78, 139.84, 138.03, 136.89, 135.12, 134.10, 133.10, 132.48, 128.48, 124.77, 124.36, 123.72, 123.54, 123.50, 31.37, 31.31, 30.03, 28.60, 22.40, 13.95 ppm. IR: $\tilde{\nu}_{\text{max}}$ = 3059.6 (w), 1595.8 (w), 1536.1 (w), 1297.8 (w), 1235.1 (w), 1209.8 (w), 1162.5 (w), 1063.5 (w), 1044.4 (m), 1001.9 (w), 909.6 (m), 865.2 (w), 791.7 (s), 737.9 (w), 723.4 (m) cm^{-1} .

Preparation of 7a: Compound **5d** (1.00 g, 1.39 mmol), PdCl_2 (0.049 g, 0.276 mmol), PPh_3 (0.146 g, 0.557 mmol) and **6** (4.51 g, 8.36 mmol) were stirred in degassed DMF (2.4 mL) at 120 °C for 16 h. After cooling to room temp., hexanes were added and the crude product (1.54 g, 1.10 mmol, 79%) was filtered and washed with hexanes. The crude material was washed with hot EtOAc and recrystallized from DCE to afford an orange microcrystalline powder (0.72 g, 0.516 mmol, 37%); m.p. >214 °C (dec.). ^1H NMR (CDCl_3 , 50 °C, 500 MHz): δ = 7.11 (s, 2 H), 6.69 (d, J = 2.9 Hz, 4 H), 6.63 (d, J = 3.1 Hz, 4 H), 6.57 (s, 4 H), 6.54 (d, J = 3.2 Hz, 4 H), 6.51 (d, J = 2.7 Hz, 4 H), 2.74 (t, J = 7.9 Hz, 8 H), 1.69 (m, J = 7.5 Hz, 8 H), 1.47–1.34 (m, 24 H), 0.96 (t, J = 6.9 Hz, 12 H) ppm. IR: $\tilde{\nu}_{\text{max}}$ = 1547.4 (w), 1530.3 (w), 1496.7 (m), 1304.5 (w), 1181.4 (w), 1054.3 (w), 852.37 (m), 785.9 (s), 722.9 (m) cm^{-1} . $\text{C}_{78}\text{H}_{74}\text{S}_{12}$: C 67.10, H 5.34; found C 66.90, H 5.13. Given the low solubility of this compound ^{13}C NMR spectroscopic analysis was not possible. The identity of this compound was confirmed by ^1H NMR spectroscopy and elemental analysis.

Preparation of 12b: 1,2,4,5-Tetrabromobenzene (0.54 g, 1.37 mmol), PdCl_2 (17 mg, 0.096 mmol), PPh_3 (50 mg, 0.191 mmol) and **11b** (4.0 g, 8.23 mmol) were stirred in degassed DMF (0.7 mL) at 140 °C for 16 h. After cooling to room temp., the crude material was dissolved in hexanes and any remaining solids were filtered off. After an aqueous work up, the organic phase was concentrated to afford the crude product as an oil. Crystallization was achieved by using EtOAc, which afforded colourless needles (0.85 g, 0.99 mmol, 72%); m.p. 58–64 °C. ^1H NMR (CDCl_3 , room temp., 400 MHz): δ = 7.55 (s, 2 H), 6.73 (d, J = 3.5 Hz, 4 H), 6.61 (d, J = 3.5 Hz, 4 H), 2.74 (t, J = 7.5 Hz, 8 H), 1.62 (m, J = 7.4 Hz, 8 H), 1.37–1.20 (m, 40 H), 0.86 (t, J = 6.9 Hz, 12 H) ppm. ^{13}C NMR (CDCl_3 , room temp., 400 MHz): δ = 146.9, 139.3, 132.9, 126.8, 123.9, 31.9, 31.7, 30.1, 29.3, 29.2, 29.1, 22.7, 14.1 ppm.

Preparation of 5b: A solution of iron(III) chloride (0.81 g, 0.495 mmol) in nitromethane (15 mL) was added dropwise to a

solution of **12b** (0.85 g, 0.01 mmol) in CH_2Cl_2 (40 mL). **Caution!** Nitromethane is an explosive liquid, which can detonate upon extreme heat. Its contact with amines, alkali metals, and strong reducing agents should be strictly avoided. After 50 min, methanol (400 mL) was added and the reaction was stirred for 45 min. The crude product was collected by filtration and washed with methanol to give the crude product (696 mg, 0.817 mmol, 83%). Recrystallization from ethyl acetate gave **5b** as a yellow microcrystalline solid (320 mg, 38%); m.p. >167 °C (dec.). ^1H NMR (CDCl_3 , room temp., 400 MHz): δ = 8.60 (s, 2 H), 7.30 (s, 4 H), 3.00 (t, J = 7.5 Hz, 8 H), 1.83 (m, J = 7.56 Hz, 8 H), 1.49–1.18 (m, 40 H), 0.88 (t, J = 6.7 Hz, 12 H) ppm. ^{13}C NMR (CDCl_3 , room temp., 400 MHz): δ = 146.3, 133.3, 133.2, 125.2, 120.2, 118.1, 31.9, 31.6, 30.9, 29.4, 29.3, 29.2, 22.7, 14.2 ppm. $\text{C}_{54}\text{H}_{74}\text{S}_4$ (851.42): calcd. C 76.18, H 8.76; found C 76.42, H 8.78.

Preparation of 6b: Compound **5d** (0.200 g, 0.278 mmol), PdCl_2 (5 mg, 0.028 mmol), PPh_3 (15 mg, 0.057 mmol) and **11b** (0.812 g, 1.67 mmol) were stirred in degassed DMF (0.1 mL) at 130 °C for 16 h. After cooling to room temp., hexanes were added and the crude product (0.240 g, 0.204 mmol, 73%) was filtered off and washed with hexanes. Recrystallization from EtOAc afforded a bright-yellow microcrystalline solid (196 mg, 0.166 mmol); crystals that were suitable for X-ray crystallography were obtained from dichloroethane; m.p. 132–141 °C. ^1H NMR (CDCl_3 , room temp., 400 MHz): δ = 7.84 (s, 2 H), 7.14 (s, 4 H), 7.00 (s, J = 3.4 Hz, 4 H), 6.65 (d, J = 3.4 Hz, 4 H), 2.81 (t, J = 7.7 Hz, 8 H), 1.73 (m, J = 7.4 Hz, 8 H), 1.48–1.28 (m, 24 H), 0.91 (t, J = 6.8 Hz, 12 H) ppm. ^{13}C NMR (CDCl_3 , room temp., 400 MHz): δ = 145.6, 137.0, 135.2, 133.2, 133.0, 124.7, 124.4, 124.0, 117.7, 117.3, 32.0, 31.6, 30.3, 29.5, 29.4, 22.8, 14.2 ppm. $\text{C}_{70}\text{H}_{82}\text{S}_8$ (1179.90): calcd. C 71.25, H 7.00; found C 71.47, H 6.91.

CCDC-939234 (for **6b**) and -939235 (for **9a**) contain the supplementary crystallographic data for this paper. These data can be obtained free of charge from The Cambridge Crystallographic Data Centre via www.ccdc.cam.ac.uk/data_request/cif.

Supporting Information (see footnote on the first page of this article): Electrochemistry, absorption and emission spectroscopy, crystallography, EHT band structures, DFT calculations, device fabrication and testing, NMR spectra.

Acknowledgments

The authors would like to thank Bobak Gholamkhash for assistance with TFT device fabrication and testing. The authors are grateful to Natural Sciences and Engineering Research Council of Canada (NSERC) for funding this work and Canada Foundation for Innovation (CFI) for the instrumentation. A. A. L. acknowledges support through an NSERC postdoctoral fellowship.

- [1] C. Wang, H. Dong, W. Hu, Y. Liu, D. Zhu, *Chem. Rev.* **2012**, *112*, 2208–2267.
- [2] a) T. Lei, J. Pei, *J. Mater. Chem.* **2012**, *22*, 785–798; b) A. Mishra, C.-Q. Ma, P. Baeuerle, *Chem. Rev.* **2009**, *109*, 1141–1276.
- [3] a) H. N. Tsao, K. Muellen, *Chem. Soc. Rev.* **2010**, *39*, 2372–2386; b) E. Gomar-Nadal, J. Puigmarti-Luis, D. B. Amabilino, *Chem. Soc. Rev.* **2008**, *37*, 490–504; c) H. Sirringhaus, P. J. Brown, R. H. Friend, M. M. Nielsen, K. Bechgaard, B. M. W. Langeveld-Voss, A. J. H. Spiering, R. A. J. Janssen, E. W. Meijer, P. Herwig, D. M. de Leeuw, *Nature* **1999**, *401*, 685–688; d) S. R. Forrest, *Nature* **2004**, *428*, 911–918; C. D. Dimitrakopoulos, P. R. L. Malenfant, *Adv. Mater.* **2002**, *14*, 99–117.

- [4] a) H. Sirringhaus, P. J. Brown, R. H. Friend, M. M. Nielsen, K. Bechgaard, B. M. W. Langeveld-Voss, A. J. H. Spiering, R. A. J. Janssen, E. W. Meijer, P. Herwig, D. M. de Leeuw, *Nature* **1999**, *401*, 685–688; b) N. S. Colella, L. Zhang, A. L. Briseno, *Mater. Matters* **2012**, *7*, 18–20; c) A. Salleo, R. J. Kline, D. M. DeLongchamp, M. L. Chabinyc, *Adv. Mater.* **2010**, *22*, 3812–3838; d) A. Salleo, *Mater. Today* **2007**, *10*, 38–45; e) T. W. Kelley, L. D. Boardman, T. D. Dunbar, D. V. Muires, M. J. Pellerite, T. Y. P. Smith, *J. Phys. Chem. B* **2003**, *107*, 5877–5881.
- [5] T. W. Kelley, L. D. Boardman, T. D. Dunbar, D. V. Muires, M. J. Pellerite, T. Y. P. Smith, *J. Phys. Chem. B* **2003**, *107*, 5877–5881.
- [6] K. Takimiya, T. Yamamoto, H. Ebata, T. Izawa, *Sci. Technol. Adv. Mater.* **2007**, *8*, 273–276.
- [7] a) K. Takimiya, S. Shinamura, I. Osaka, E. Miyazaki, *Adv. Mater.* **2011**, *23*, 4347–4370; b) J. E. Anthony, *Chem. Rev.* **2006**, *106*, 5028–5048; c) J. E. Anthony, *Angew. Chem.* **2008**, *120*, 460; *Angew. Chem. Int. Ed.* **2008**, *47*, 452–483; d) M. J. Kang, I. Doi, H. Mori, E. Miyazaki, K. Takimiya, M. Ikeda, H. Kuwbara, *Adv. Mater.* **2011**, *23*, 1222–1225; e) A. N. Sokolov, S. Atahan-Evrenk, R. Mondal, H. B. Akkerman, R. S. Sanchez-Carrera, S. Granados-Focil, J. Schrier, S. C. B. Mannsfeld, A. P. Zoombelt, Z. Bao, A. Aspuru-Guzik, *Nat. Commun.* **2011**, *2*, 437.
- [8] D. F. Perepichka, F. Rosei, *Science* **2009**, *323*, 216–217.
- [9] F. He, W. Wang, W. Chen, T. Xu, S. B. Darling, J. Strzalka, Y. Liu, L. Yu, *J. Am. Chem. Soc.* **2011**, *133*, 3284–3287.
- [10] A. L. Kanibolotsky, I. F. Perepichka, P. J. Skabara, *Chem. Soc. Rev.* **2010**, *39*, 2695–2728.
- [11] J. Wang, H. Xu, B. Li, X.-P. Cao, H.-L. Zhang, *Tetrahedron* **2012**, *68*, 1192–1197.
- [12] a) J. Cremer, P. Bauerle, *J. Mater. Chem.* **2006**, *16*, 874–884; b) Z.-F. Duan, X.-Q. Huang, Z.-G. Yang, D. Hoshino, S. Kitanaka, G.-Y. Zhao, Y. Nishioka, *Molecules* **2011**, *16*, 4467–4481; c) H. T. Black, S. Liu, V. S. Ashby, *Org. Lett.* **2011**, *13*, 6492–6495; d) H. Shang, H. Fan, Y. Liu, W. Hu, Y. Li, X. Zhan, *Adv. Mater.* **2011**, *23*, 1554–1557; e) L. Chen, P. Li, Y. Cheng, Z. Xie, L. Wang, X. Jing, F. Wang, *Adv. Mater.* **2011**, *23*, 2986–2990.
- [13] Y. Nicolas, P. Blanchard, E. Levillain, M. Allain, N. Mercier, J. Roncali, *Org. Lett.* **2004**, *6*, 273–276.
- [14] J. L. Brusso, O. D. Hirst, A. Dadvand, S. Ganesan, F. Cicoira, C. M. Robertson, R. T. Oakley, F. Rosei, D. F. Perepichka, *Chem. Mater.* **2008**, *20*, 2484–2494.
- [15] A. A. Leitch, A. Mansour, K. A. Stobo, I. Korobkov, J. L. Brusso, *Cryst. Growth Des.* **2012**, *12*, 1416–1421.
- [16] a) W.-J. Liu, Y. Zhou, Y. Ma, Y. Cao, J. Wang, J. Pei, *Org. Lett.* **2007**, *9*, 4187–4190; b) R. Gutzler, O. Ivashenko, C. Fu, J. L. Brusso, F. Rosei, D. F. Perepichka, *Chem. Commun.* **2011**, *47*, 9453–9455; c) C. Fu, F. Rosei, D. F. Perepichka, *ACS Nano* **2012**, *6*, 7973–7980; d) L. E. Dinca, C. Y. Fu, J. M. MacLeod, J. Lipton-Duffin, J. L. Brusso, C. E. Szakacs, D. L. Ma, D. F. Perepichka, F. Rosei, *ACS Nano* **2013**, *7*, 1652–1657.
- [17] L. Zoephel, V. Enkelmann, R. Rieger, K. Muellen, *Org. Lett.* **2011**, *13*, 4506–4509.
- [18] a) J. Luo, B. M. Zhao, H. S. O. Chan, C. Y. Chi, *J. Mater. Chem.* **2010**, *20*, 1932–1941; b) Y. Zhou, W. J. Liu, W. Zhang, X. Y. Cao, Q. F. Zhou, Y. G. Ma, J. Pei, *J. Org. Chem.* **2006**, *71*, 6822–6828.
- [19] a) B. S. Jensen, V. D. Parker, *J. Am. Chem. Soc.* **1975**, *97*, 5211–5217; b) A. Rainis, M. Szwarc, *J. Am. Chem. Soc.* **1974**, *96*, 3008–3010.
- [20] R. T. Boere, K. H. Mook, M. Parvez, *Z. Anorg. Allg. Chem.* **1994**, *620*, 1589–1598.
- [21] Y. He, W. Wu, G. Zhao, Y. Liu, Y. Li, *Macromolecules* **2008**, *41*, 9760–9766.
- [22] T. M. Barclay, A. W. Cordes, C. D. MacKinnon, R. T. Oakley, R. W. Reed, *Chem. Mater.* **1997**, *9*, 981–990.
- [23] X. N. Zhang, A. J. Matzger, *J. Org. Chem.* **2003**, *68*, 9813–9815.
- [24] J. Wang, H. Xu, B. Li, X.-P. Cao, H.-L. Zhang, *Tetrahedron* **2012**, *68*, 1192–1197.
- [25] Y. V. Zefirov, P. M. Zorkii, *Zh. Strukt. Khim.* **1976**, *17*, 745–756.
- [26] R. C. Haddon, A. P. Ramirez, S. H. Glarum, *Adv. Mater.* **1994**, *6*, 316–321.
- [27] R. C. Haddon, T. Siegrist, R. M. Fleming, P. M. Bridenbaugh, R. A. Laudise, *J. Mater. Chem.* **1995**, *5*, 1719–1724.
- [28] V. C. Sundar, J. Zaumseil, V. Podzorov, E. Menard, R. L. Willett, T. Someya, M. E. Gershenson, J. A. Rogers, *Science* **2004**, *303*, 1644–1646.
- [29] a) F. Cicoira, J. A. Miwa, D. F. Perepichka, F. Rosei, *J. Phys. Chem. A* **2007**, *111*, 12674–12678; b) M. C. Blum, E. Cavar, M. Pivetta, F. Patthey, W. D. Schneider, *Angew. Chem.* **2005**, *117*, 5468; *Angew. Chem. Int. Ed.* **2005**, *44*, 5334–5337.
- [30] G. Barbarella, L. Favaretto, G. Sotgiu, M. Zambianchi, L. Antolini, O. Pudova, A. Bongini, *J. Org. Chem.* **1998**, *63*, 5497–5506.
- [31] M. Melucci, G. Barbarella, M. Zambianchi, M. Benzi, F. Biscarini, M. Cavallini, A. Bongini, S. Fabbroni, M. Mazzeo, M. Anni, G. Gigli, *Macromolecules* **2004**, *37*, 5692–5702.
- [32] S. Cheng, D. Shen, X. Zhu, X. Tian, D. Zhou, L.-J. Fan, *Eur. Polym. J.* **2009**, *45*, 2767–2778.
- [33] *APEX Software Suite*, v. 2010, Bruker AXS, Madison, WI, **2005**.

Received: May 17, 2013

Published Online: ■